Integrated Real-time Economic Dispatch and Optimal Automatic Generation Control

Kamlesh Sawant*, Bijit Kumar Dey*, Emiliano Dall'Anese⋆, Deepak Ramasubramanian‡, Sairaj Dhople*
*Electrical and Computer Engineering, University of Minnesota, Minneapolis, MN, United States
⋆Department of Electrical and Computer Engineering, Boston University, Boston, MA, United States
‡Transmission Operations & Planning, Electric Power Research Institute, Knoxville, TN, United States
Emails: sawan035@umn.edu, dey00032@umn.edu, edallane@bu.edu, dramasubramanian@epri.com, sdhople@umn.edu

***Abstract*—In this paper, we propose a control architecture for a single-area power system that integrates economic dispatch (ED) and automatic generation control (AGC) through a continuous-time feedback loop. The AGC state is incorporated into the ED optimization problem as a proxy for real-time net load to achieve economic efficiency and frequency regulation simultaneously. We put forth a continuous-time controller that solves this integrated ED–AGC optimization problem in real-time, and show that the equilibria of these dynamics satisfy the Karush-Kuhn-Tucker (KKT) optimality conditions. We also establish stability guarantees using the Lur'e system framework based on linear matrix inequalities (LMIs). The efficacy of the proposed control architecture is established through a 14-bus simulation in MATLAB. Simulation results show that the system with the proposed control architecture maintains economic optimality in steady state while tracking real-time load changes.**

***Index Terms*—Automatic generation control, constrained optimization, economic dispatch, real-time optimization.**

I. Introduction

Contemporary power grids face increasing uncertainty due to high integration of renewable generation and the rapid growth of dynamic loads such as data centers. These sources and loads introduce variability in both power production and demand. Grid control remains organized hierarchically across different time scales: tertiary control (economic dispatch, ED) updates generation setpoints every 5 minutes or more using load forecasts to minimize operating costs, while secondary control (automatic generation control, AGC) acts every few seconds to maintain frequency stability [1]. Conventional AGC schemes distribute regulation effort through fixed participation factors that ignore real-time economic objectives. As a result, forecast inaccuracies force AGC to make sizable corrective actions, driving generators away from their economically optimal operating points. This leads to cost-inefficient operation unless specific tuning guidelines are enforced [2], [3].

Several innovations have been proposed to the hierarchical control layers of the power-systems operational stack to enhance dynamic and economic performance [4]. A short survey of pertinent literature follows next. Dynamics corresponding to AGC have been incorporated as constraints in the ED formulation to improve frequency regulation [5]. A continuous-time ED, intended for realization in near real time, is put forth in [6]; the solution strategy yields continuous trajectories rather than discontinuous setpoints. Other formulations introduce an explicit AGC state representing total generation within each control area to economically allocate AGC power among participating generators [7]. In a similar vein, the unification of ED and AGC through optimization-based decomposition, which co-optimizes economic efficiency and frequency regulation, has been studied in [1] and [2]. Specifically, the unified ED–AGC optimal control problem is decomposed into two coupled optimization problems: an ED problem and an optimal AGC problem that utilizes the AGC state and ED outputs to determine the real-time economic allocation of AGC power [2].

In this paper, we present a single optimization problem for frequency regulation and resource allocation that merges the ED and AGC layers. Motivated by the approach in [2], we formulate an optimal ED–AGC problem for a single-area power system that incorporates the AGC state within its constraints as a proxy for real-time load to achieve both economic efficiency and frequency regulation simultaneously. We propose continuous-time dynamics that accommodate various controllers incorporating integral and proportional actions to solve the optimal ED–AGC problem in real-time. We show that the equilibria of the dynamics satisfy the Karush-Kuhn-Tucker (KKT) optimality conditions and analyze closed-loop stability within the Lur'e system framework using linear matrix inequality (LMI) criteria. Finally, numerical results for a 14-bus system validate stability via LMI conditions and show that the system achieves steady-state economic optimality and frequency regulation through time-domain simulations.

II. Power system dynamics

We consider an AC power network with buses indexed by the set $\mathcal{N} = \{1, \dots, N\}$ under a hierarchical control architecture comprising primary, secondary, and tertiary control. Each bus, $k \in \mathcal{N}$, is associated with a phase angle relative to the reference bus, θ_k, aggregate generation, p_k, demand, d_k, and deviation from nominal frequency, denoted ω_k. Let $\mathbf{p}, \mathbf{d}, \boldsymbol{\omega} \in \mathbb{R}^N$ and $\boldsymbol{\theta} \in \mathbb{R}^{N-1}$ denote the vectors stacking these quantities. Pertinent dynamics at this primary-frequency regulation level are given by:

$$\dot{\boldsymbol{\theta}} = \mathbf{T}_{-1}\boldsymbol{\omega}, \tag{1a}$$

$$\mathbf{M}\dot{\boldsymbol{\omega}} = \mathbf{p} - \mathbf{d} - \mathbf{D}\boldsymbol{\omega} - \mathbf{B}\mathbf{T}_0\boldsymbol{\theta}, \tag{1b}$$

$$\boldsymbol{\Gamma}\dot{\mathbf{p}} = \mathbf{p}^{\mathrm{ref}} - \mathbf{p} + \mathbf{R}\boldsymbol{\omega}, \tag{1c}$$

979-8-3315-8138-1

where $\mathbf{T}_{-1} = \begin{bmatrix}\mathbf{I}_{N-1} & -\mathbb{1}_{N-1}\end{bmatrix}$ and $\mathbf{T}_0 = \begin{bmatrix}\mathbf{I}_{N-1} & \mathbf{0}\end{bmatrix}^\top$. With regard to notation, bold letters denote matrices and vectors; $\mathbf{I}$, $\mathbf{0}$, and $\mathbb{1}$ denote the identity matrix, the zero matrix/vector, and the vector of ones. We omit matrix and vector dimensions when they can be inferred from the context. Matrices $\mathbf{M}, \mathbf{D}, \mathbf{\Gamma}$, and $\mathbf{R} \in \mathbb{R}^{N\times N}$ are diagonal matrices of bus inertia, damping constants, governor time constants, and frequency-power droop slopes, respectively; $\mathbf{B} \in \mathbb{R}^{N\times N}$ is the DC power-flow susceptance matrix, and $\mathbf{p}^{\mathrm{ref}} \in \mathbb{R}^N$ are commanded power references received from secondary control [8].

At the secondary layer, AGC receives setpoints $\mathbf{p}^\star \in \mathbb{R}^N$ from tertiary control and generates power references $\mathbf{p}^{\mathrm{ref}} \in \mathbb{R}^N$ as $\mathbf{p}^{\mathrm{ref}} = \mathbf{p}^\star + \boldsymbol{\alpha}(z - \mathbb{1}^\top \mathbf{p}^\star)$. Here, $\boldsymbol{\alpha} \in \mathbb{R}^N$ contains participation factors of resources under the control of AGC. The variable $z \in \mathbb{R}$ is the AGC state that tracks the real-time generation to meet net load, governed by the dynamics:

$$\tau_{\mathrm{z}}\dot{z} = -z - \mathrm{ACE} + \mathbb{1}^\top \mathbf{p}, \tag{2}$$

where $\tau_{\mathrm{z}} \in \mathbb{R}$ is the AGC time constant. The term $\mathrm{ACE} \in \mathbb{R}$ is the Area Control Error that captures frequency error associated with the area, given by $\mathrm{ACE} = -\beta\boldsymbol{\omega}_{\mathrm{area}}$ where $\beta \in \mathbb{R}_{<0}$ is an area bias factor and $\boldsymbol{\omega}_{\mathrm{area}} = (\mathbb{1}^\top/N)\boldsymbol{\omega}$ is the averaged frequency of resources of the area [9].

The dynamics (1)–(2) can be expressed in state-space form:

$$\dot{\mathbf{x}}_{\mathrm{p}} = \mathbf{A}_{\mathrm{p}}\mathbf{x}_{\mathrm{p}} + \mathbf{B}_{\mathrm{p}}\mathbf{u}_{\mathrm{p}}, \tag{3}$$

with $\mathbf{x}_{\mathrm{p}} = \begin{bmatrix}\boldsymbol{\theta}^\top & \boldsymbol{\omega}^\top & \mathbf{p}^\top & z\end{bmatrix}^\top \in \mathbb{R}^{3N}, \mathbf{u}_{\mathrm{p}} = \begin{bmatrix}\mathbf{p}^{\star\top} & \mathbf{d}^\top\end{bmatrix}^\top \in \mathbb{R}^{2N}$. Under the assumption that $\mathbb{1}^\top\boldsymbol{\alpha} = 1$, the system dynamics (1)–(2) converge to the steady state: $\overline{\boldsymbol{\omega}} = \mathbf{0}, \mathbb{1}^\top\overline{\mathbf{p}} = \overline{z} = \mathbb{1}^\top\mathbf{d}$, i.e., the AGC state z tracks the total load demand $\mathbb{1}^\top\mathbf{d}$ at steady state [10, Lem. 1]. This motivates the integrated optimal ED–AGC formulation that follows.

III. Control Architecture

A. Conventional Economic Dispatch

The conventional hierarchical control architecture, shown in Fig. 1(left), operates with unidirectional information flow where ED provides setpoints to AGC based on load forecast, δ. With complete information about the load available at hand, it would be reasonable to set $\delta = \mathbb{1}^\top\mathbf{d}$, but this is not generally feasible due to forecasting errors and the inability to monitor load in real time. The conventional resource-allocation problem for ED reads:

$$\underset{\boldsymbol{\rho}\in\mathbb{R}^N}{\text{minimize}} \quad \tfrac{1}{2}\boldsymbol{\rho}^\top\mathbf{Q}\boldsymbol{\rho} + \mathbf{q}^\top\boldsymbol{\rho} \tag{4a}$$

$$\text{subject to} \quad \mathbb{1}^\top\boldsymbol{\rho} = \delta, \; \boldsymbol{\rho}^{\min} \leq \boldsymbol{\rho} \leq \boldsymbol{\rho}^{\max}, \tag{4b}$$

where (4b) ensures supply-demand balance and generation capacity limits. Matrix $\mathbf{Q}$ is assumed to be positive definite ($\mathbf{Q} \succ \mathbf{0}$), ensuring the cost (4a) is strongly convex [11, Sec. 3.1.4].

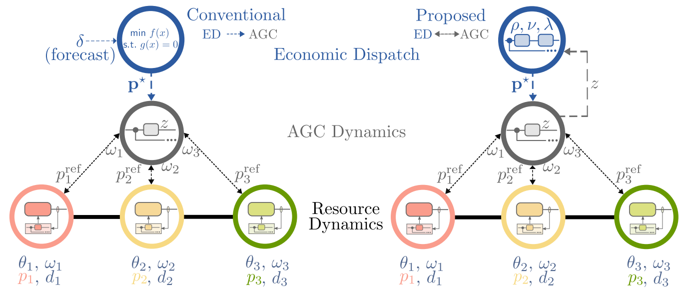

Fig. 1: (Left) Conventional hierarchical architecture with unidirectional information flow (ED $\rightarrow$ AGC). (Right) Proposed integrated architecture with feedback, where AGC state z provides real-time demand information to ED (ED $\leftrightarrow$ AGC).

B. Proposed Integrated Optimal ED–AGC

In contrast to the conventional approach, the proposed architecture establishes feedback as depicted in Fig. 1(right), with the AGC state z serving as an estimate for real-time demand in the ED resource allocation problem. We create this feedback interconnection by substituting $\delta = z$ in (4b) as a suitable proxy for the net load $\mathbf{1}^\top\mathbf{d}$. While $\mathbf{d}$ is an exogenous disturbance that cannot be measured in real-time, the steady-state value of z tracks it. With such an architecture, the resource allocation problem reads:

$$\underset{\boldsymbol{\rho}\in\mathbb{R}^N}{\text{minimize}} \quad \tfrac{1}{2}\boldsymbol{\rho}^\top\mathbf{Q}\boldsymbol{\rho} + \mathbf{q}^\top\boldsymbol{\rho} \tag{5a}$$

$$\text{subject to} \quad \mathbb{1}^\top\boldsymbol{\rho} = z, \; \begin{bmatrix}-\mathbf{I}\\ \mathbf{I}\end{bmatrix}\boldsymbol{\rho} - \begin{bmatrix}-\boldsymbol{\rho}^{\min}\\ \boldsymbol{\rho}^{\max}\end{bmatrix} \leq \mathbf{0}, \tag{5b}$$

where $z \in \mathbb{R}$ is the AGC state variable, and the constraints are rewritten to facilitate forthcoming developments. The inequality constraints can be expressed as $\mathbf{H}\boldsymbol{\rho} - \mathbf{h} \leq \mathbf{0}$, where $\mathbf{H} \in \mathbb{R}^{2N\times N}$ and $\mathbf{h} \in \mathbb{R}^{2N}$. The Lagrangian $\mathcal{L}(\boldsymbol{\rho}, \nu, \boldsymbol{\lambda}) : \mathbb{R}^N \times \mathbb{R} \times \mathbb{R}^{2N} \to \mathbb{R}$ for the above problem is given by

$$\mathcal{L}(\boldsymbol{\rho}, \nu, \boldsymbol{\lambda}) = C(\boldsymbol{\rho}) + \nu^\top(\mathbb{1}^\top\boldsymbol{\rho} - z) + \boldsymbol{\lambda}^\top(\mathbf{H}\boldsymbol{\rho} - \mathbf{h}), \tag{6}$$

where $\nu \in \mathbb{R}$ and $\boldsymbol{\lambda} \in \mathbb{R}^{2N}$ are the Lagrange multipliers.

We assume the feasible set $\Omega(z) := \{\boldsymbol{\rho} \in \mathbb{R}^N \mid \mathbb{1}^\top\boldsymbol{\rho} - z = 0, \mathbf{H}\boldsymbol{\rho} - \mathbf{h} \leq \mathbf{0}\}$ is non-empty for every $z \in \mathcal{Z}$ in a compact set $\mathcal{Z} \subset \mathbb{R}$. Under Linear Independence Constraint Qualification (LICQ), the KKT conditions are first-order necessary conditions for optimality [12, Chap. 12]. The LICQ holds automatically for (5) since the lower and upper bounds cannot be simultaneously active. The KKT conditions for problem (5) at $(\boldsymbol{\rho}^\star, \nu^\star, \boldsymbol{\lambda}^\star)$ for each $z \in \mathcal{Z}$ are:

$$\mathbf{Q}\boldsymbol{\rho}^\star + \mathbf{q} + \mathbb{1}\nu^\star + \mathbf{H}^\top\boldsymbol{\lambda}^\star = \mathbf{0}, \tag{7a}$$

$$\mathbb{1}^\top\boldsymbol{\rho}^\star - z = 0 \text{ and } \mathbf{H}\boldsymbol{\rho}^\star - \mathbf{h} \leq \mathbf{0}, \tag{7b}$$

$$\boldsymbol{\lambda}^\star \geq \mathbf{0}, \tag{7c}$$

$$\boldsymbol{\lambda}^\star \circ (\mathbf{H}\boldsymbol{\rho}^\star - \mathbf{h}) = \mathbf{0}, \tag{7d}$$

where $\circ$ denotes element-wise product. Given non-empty feasibility and $\mathbf{Q} \succ \mathbf{0}$ assumptions, problem (5) admits a unique global minimizer $\boldsymbol{\rho}^\star$ with unique optimal Lagrange multipliers $\nu^\star$ and $\boldsymbol{\lambda}^\star$ [12, Sec. 12.3]. In this case, the KKT conditions (7) are necessary and sufficient for optimality at $(\boldsymbol{\rho}^\star, \nu^\star, \boldsymbol{\lambda}^\star)$ [11, Sec 5.5.3]. Since the constraints in (5) are linear, the assumption of non-empty feasibility implies that the problem satisfies Slater's constraint qualification [11, Sec. 5.2.3]. Equivalently, with Slater's condition satisfied, $(\boldsymbol{\rho}^\star, \nu^\star, \boldsymbol{\lambda}^\star)$ corresponds to a saddle point of the Lagrangian (6) [11, Sec. 5.4], satisfying

$$\mathcal{L}(\boldsymbol{\rho}^\star, \nu, \boldsymbol{\lambda}) \leq \mathcal{L}(\boldsymbol{\rho}^\star, \nu^\star, \boldsymbol{\lambda}^\star) \leq \mathcal{L}(\boldsymbol{\rho}, \nu^\star, \boldsymbol{\lambda}^\star). \tag{8}$$

The KKT conditions in (7) motivate the continuous-time dynamics formulation to solve the optimization problem (5). We discuss this next.

C. Continuous-time Optimization Dynamics

We formulate continuous-time dynamics for the primal variable $\boldsymbol{\rho}$ to solve (5) such that equilibria of the dynamics satisfy the KKT stationarity condition (7a):

$$\dot{\boldsymbol{\rho}} = -\gamma_\rho \left(\mathbf{Q}\boldsymbol{\rho} + \mathbf{q} + \begin{bmatrix} \mathbb{1} & \mathbf{H}^\top \end{bmatrix} \begin{bmatrix} \nu \\ \boldsymbol{\lambda} \end{bmatrix} \right), \tag{9}$$

where $\gamma_\rho \in \mathbb{R}_{>0}$. In what follows, we describe different controllers to generate the dual variables ν and $\boldsymbol{\lambda}$ in (9), ensuring the remaining KKT conditions—primal feasibility (7b), dual feasibility (7c), and complementary slackness (7d)—are satisfied at steady state. Consider $\mathcal{C} \in \{\nu, \boldsymbol{\lambda}\}$ as an index representing either the ν-controller or the $\boldsymbol{\lambda}$-controller. Then, the controller dynamics associated with the dual variables ν and $\boldsymbol{\lambda}$ are represented in state-space form as:

$$\dot{\mathbf{x}}_\mathcal{C} = \mathbf{A}_\mathcal{C}\mathbf{x}_\mathcal{C} + \mathbf{B}_\mathcal{C}\left(\mathbf{u}_\mathcal{C} + \boldsymbol{\Psi}_\mathcal{C}\right), \tag{10a}$$

$$\mathbf{y}_\mathcal{C} = \mathbf{C}_\mathcal{C}\mathbf{x}_\mathcal{C} + \mathbf{D}_\mathcal{C}\mathbf{u}_\mathcal{C}, \tag{10b}$$

where the controller's input are $\mathbf{u}_\nu = \mathbb{1}^\top\boldsymbol{\rho} - z \in \mathbb{R}$ and $\mathbf{u}_{\boldsymbol{\lambda}} = \mathbf{H}\boldsymbol{\rho} - \mathbf{h} \in \mathbb{R}^{2N}$ for the two cases, and anti-windup term $\boldsymbol{\Psi}_\nu = 0$ and $\boldsymbol{\Psi}_{\boldsymbol{\lambda}} = \mu(\mathbf{max}(\mathbf{0}, \mathbf{y}_{\boldsymbol{\lambda}}) - \mathbf{y}_{\boldsymbol{\lambda}})$ with $\mu \in \mathbb{R}_{>0}$. Here $\mathbf{max}(\mathbf{0}, \cdot)$ denotes element-wise maximum. These primal-dual gradient-flow dynamics (9)–(10) seek the saddle point characterized by (8) and asymptotically enforce the generation limits $\boldsymbol{\rho}^{\min}$ and $\boldsymbol{\rho}^{\max}$. Similar strategies have been reported in previous studies [13]–[16].

For the closed-loop system (9)–(10) with dual variables $\nu = y_\nu$ and $\boldsymbol{\lambda} = \mathbf{max}(\mathbf{0}, \mathbf{y}_{\boldsymbol{\lambda}})$, suppose $\mathbf{A}_\nu = \mathbf{0}, \mathbf{A}_{\boldsymbol{\lambda}} = \mathbf{0}$, and $\mathbf{B}_\nu$, $\mathbf{B}_{\boldsymbol{\lambda}}$ have full column rank. Then any equilibrium point $(\overline{\boldsymbol{\rho}}, \overline{\nu}, \overline{\boldsymbol{\lambda}})$ satisfies the KKT conditions (7). To see this, note that setting $\dot{\mathbf{x}}_\nu = \mathbf{0}$ and $\dot{\mathbf{x}}_{\boldsymbol{\lambda}} = \mathbf{0}$ yields $\mathbf{1}^\top\overline{\boldsymbol{\rho}} - z = 0$ and $\mathbf{H}\overline{\boldsymbol{\rho}} - \mathbf{h} = -\mu\ (\mathbf{max}(\mathbf{0}, \overline{\mathbf{y}}_{\boldsymbol{\lambda}}) - \overline{\mathbf{y}}_{\boldsymbol{\lambda}}) = \mu\ \mathbf{min}(\mathbf{0}, \overline{\mathbf{y}}_{\boldsymbol{\lambda}}) \leq \mathbf{0}$ at equilibrium, satisfying primal feasibility (7b). Dual feasibility (7c) follows directly from $\overline{\boldsymbol{\lambda}} = \mathbf{max}(\mathbf{0}, \overline{\mathbf{y}}_{\boldsymbol{\lambda}}) \geq \mathbf{0}$. Moreover, complementary slackness (7d) holds since $\overline{\boldsymbol{\lambda}} \circ (\mathbf{H}\overline{\boldsymbol{\rho}} - \mathbf{h}) = \mathbf{max}(\mathbf{0}, \overline{\mathbf{y}}_{\boldsymbol{\lambda}}) \circ \mu\ \mathbf{min}(\mathbf{0}, \overline{\mathbf{y}}_{\boldsymbol{\lambda}}) = \mathbf{0}$. Finally, to verify stationarity, the equilibria $\overline{\boldsymbol{\rho}}$ obtained by substituting $\dot{\boldsymbol{\rho}} = \mathbf{0}$ in (9) satisfy stationarity (7a).

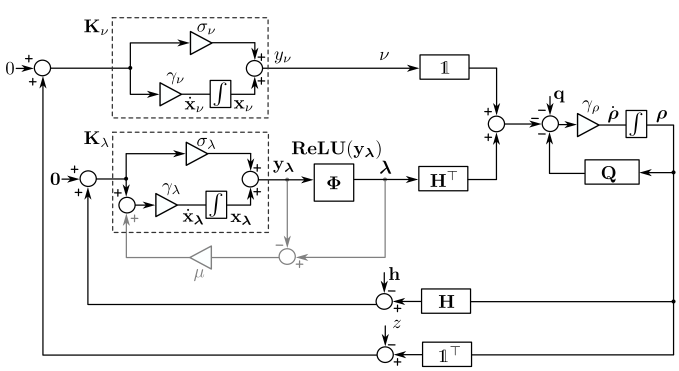

Fig. 2: Block diagram representation of the continuous-time dynamics (9)–(10) to solve (5) with the linear controllers $\mathbf{K}_\nu$ and $\mathbf{K}_\lambda$. In this instance, both controllers are PI controllers. The nonlinearity $\boldsymbol{\Phi} = \mathbf{ReLU}(.) = \mathbf{max}(\mathbf{0}, \cdot)$, along with the controller $\mathbf{K}_\lambda$, enforces the inequality constraints. The anti-windup mechanism is indicated by gray lines and parameterized by μ.

D. Representative Controller Structures

We present representative controllers for the dual dynamics (10) that, alongside the primal dynamics (9), solve problem (5). These dynamics with the representative controller structures presented below can be realized as analog circuits for real-time implementation [17].

1) Integral Action-Based Controller: Consider a Proportional-Integral (PI) controller defined by $\mathbf{A}_\mathcal{C} = \mathbf{0}, \mathbf{B}_\mathcal{C} = \gamma_\mathcal{C}\mathbf{I}, \mathbf{C}_\mathcal{C} = \mathbf{I}, \mathbf{D}_\mathcal{C} = \sigma_\mathcal{C}\mathbf{I}$, where $\gamma_\mathcal{C}, \sigma_\mathcal{C} \in \mathbb{R}_{>0}$ (see Fig. 2). The dynamics (9)–(10) with this controller satisfy the KKT conditions (7). These primal-dual dynamics are equivalent to the augmented Lagrangian method in [18] when the anti-windup parameter $\mu = 1/\sigma_{\boldsymbol{\lambda}}$. In the limit $\mu \to +\infty$, these dynamics also approximate the projected gradient-flow dynamics [19]. An integral controller (I) [20] can be obtained as a special case by setting $\sigma_\mathcal{C} = 0$.

2) Proportional Action-Based Controller: A proportional (P) controller defined by $\mathbf{A}_\mathcal{C} = \mathbf{B}_\mathcal{C} = \mathbf{C}_\mathcal{C} = \mathbf{0}, \mathbf{D}_\mathcal{C} = \sigma_\mathcal{C}\mathbf{I}$ yields dynamics (9)–(10) that do not satisfy KKT conditions (7). However, these dynamics behave as a penalty method, and as $\sigma_\mathcal{C} \to +\infty$, the equilibrium point $(\overline{\boldsymbol{\rho}}, \overline{\nu}, \overline{\boldsymbol{\lambda}})$ approaches an optimal solution that satisfies the KKT conditions [12, Sec. 17.1]. Similarly, a Lead/Lag controller with $\mathbf{A}_\mathcal{C} = -p_\mathcal{C}\mathbf{I}, \mathbf{B}_\mathcal{C} = \mathbf{I}, \mathbf{C}_\mathcal{C} = G_\mathcal{C}(z_\mathcal{C} - p_\mathcal{C})\mathbf{I}, \mathbf{D}_\mathcal{C} = G_\mathcal{C}\mathbf{I}$, where $G_\mathcal{C}, z_\mathcal{C}, p_\mathcal{C} \in \mathbb{R}_{>0}$, exhibits similar steady-state behavior to the proportional controller with effective gain corresponding to $\sigma_\mathcal{C} = (G_\mathcal{C} \times z_\mathcal{C})/p_\mathcal{C}$ [17]. Since neither proportional nor lead/lag controllers involve integrator states, the anti-windup mechanism is not necessary, i.e., $\mu = 0$.

IV. Stability Analysis

We analyze stability using tools from Lur'e systems; in fact, the system dynamics consist of a linear time-invariant (LTI) system interconnected in feedback with a sector-bounded nonlinearity. Denote $\boldsymbol{\xi} = [\mathbf{x}_\mathrm{p}^\top\ \boldsymbol{\rho}^\top\ \mathbf{x}_\nu^\top\ \mathbf{x}_{\boldsymbol{\lambda}}^\top]^\top$ and with the change of coordinates $\widetilde{\boldsymbol{\xi}} = \boldsymbol{\xi} - \overline{\boldsymbol{\xi}}$, the dynamics take the form:

$$\dot{\widetilde{\boldsymbol{\xi}}} = \mathbf{A}_{\boldsymbol{\xi}}\widetilde{\boldsymbol{\xi}} + \mathbf{B}_\mathbf{u}\widetilde{\boldsymbol{\Phi}}(\widetilde{\mathbf{y}}) + \mathbf{B}_\mathbf{d}\widetilde{\mathbf{d}}, \tag{11a}$$

$$\widetilde{\mathbf{y}} = \mathbf{C}_{\boldsymbol{\xi}}\widetilde{\boldsymbol{\xi}},\ \widetilde{z} = \mathbf{C}_\mathbf{d}\widetilde{\boldsymbol{\xi}}. \tag{11b}$$

For any initial condition $\widetilde{\boldsymbol{\xi}}(\mathbf{0})$, (11) is well-posed as the vector field is globally Lipschitz continuous [21, Thm. 3.2]. The matrices $\mathbf{A}_{\boldsymbol{\xi}}$, $\mathbf{B}_{\mathbf{u}}$, $\mathbf{B}_{\mathbf{d}}$, $\mathbf{C}_{\boldsymbol{\xi}}$, and $\mathbf{C}_{\mathbf{d}}$ are formed by combining the plant dynamics (3) with $\mathbf{p}^\star = \boldsymbol{\rho}$, primal dynamics (9), and dual dynamics (10). Their dimensions are appropriately defined based on the controller structures in Section III-D. The input $\widetilde{\mathbf{u}} = \widetilde{\boldsymbol{\Phi}}(\widetilde{\mathbf{y}}) \in \mathbb{R}^{2N}$ is injected in positive feedback via modified nonlinearity $\widetilde{\boldsymbol{\Phi}}(\widetilde{\mathbf{y}}) = \boldsymbol{\Phi}(\widetilde{\mathbf{y}} + \overline{\mathbf{y}}_{\boldsymbol{\lambda}}) - \boldsymbol{\Phi}(\overline{\mathbf{y}}_{\boldsymbol{\lambda}})$, with $\overline{\mathbf{y}}_{\boldsymbol{\lambda}}$ denoting the equilibrium value of $\mathbf{y}_{\boldsymbol{\lambda}}$, and $\widetilde{\mathbf{d}} \in \mathbb{R}^N$ is the load disturbance. The nonlinearity $\widetilde{\boldsymbol{\Phi}}(\widetilde{\mathbf{y}})$ is element-wise sector-bounded in $[0, 1]$ with $\widetilde{\boldsymbol{\Phi}}(\mathbf{0}) = \mathbf{0}$.

A. LMI-Based Stability and Performance Criteria

We now present stability criteria for the Lur'e system (11). We assume that $\mathbf{A}_{\boldsymbol{\xi}}$ is Hurwitz, which is verified numerically in Section V. Given the feasibility assumption (that $\Omega(z)$ is non-empty) and that $\mathbf{Q} \succ \mathbf{0}$, if there exists a radially unbounded quadratic Lyapunov function $V(\widetilde{\boldsymbol{\xi}}) = \widetilde{\boldsymbol{\xi}}^\top \mathbf{P} \widetilde{\boldsymbol{\xi}}$, where $\mathbf{P} = \mathbf{P}^\top \succ \mathbf{0}$ satisfies the LMI:

$$\begin{bmatrix} \mathbf{P}\mathbf{A}_{\boldsymbol{\xi}} + \mathbf{A}_{\boldsymbol{\xi}}^\top \mathbf{P} & \mathbf{P}\mathbf{B}_{\mathbf{u}} \\ \mathbf{B}_{\mathbf{u}}^\top \mathbf{P} & \mathbf{0} \end{bmatrix} + \begin{bmatrix} \mathbf{C}_{\boldsymbol{\xi}}^\top & \mathbf{0} \\ \mathbf{0} & \mathbf{I} \end{bmatrix} \boldsymbol{\Pi} \begin{bmatrix} \mathbf{C}_{\boldsymbol{\xi}} & \mathbf{0} \\ \mathbf{0} & \mathbf{I} \end{bmatrix} \prec \mathbf{0}, \tag{12}$$

where $\boldsymbol{\Pi} = \begin{bmatrix} \mathbf{0} & \mathbf{I} \\ \mathbf{I} & -2\mathbf{I} \end{bmatrix}$ is the multiplier for sector-bounded nonlinearities in $[0, 1]$, then, the system (11) is: (i) globally asymptotically stable if (12) holds, and globally exponentially stable with rate κ if (12) holds with $\mathbf{A}_{\boldsymbol{\xi}}$ replaced by $\mathbf{A}_{\boldsymbol{\xi}} + \kappa\mathbf{I}$ for some $\kappa \in \mathbb{R}_{>0}$ [22, Thm. 3]; (ii) Lyapunov stable if (12) holds with non-strict inequality ($\preceq \mathbf{0}$) [22, Thm. 1].

We next establish a bound on the induced L_2 gain γ from the load disturbance $\widetilde{\mathbf{d}}$ to the AGC state $\widetilde{z}$, selected as the performance output, such that $\|\widetilde{z}\|_{L_2} \le \gamma \|\widetilde{\mathbf{d}}\|_{L_2}$. Consider the system (11) with sector-bounded nonlinearity $\widetilde{\boldsymbol{\Phi}}(\widetilde{\mathbf{y}}) \in [0, 1]$. If there exists a matrix $\mathbf{P} = \mathbf{P}^\top \succ \mathbf{0}$, and $\eta \in \mathbb{R}_{\ge 0}$ and $\gamma \in \mathbb{R}_{>0}$ such that the following LMI holds:

$$\begin{bmatrix} \mathbf{A}_{\boldsymbol{\xi}}^\top \mathbf{P} + \mathbf{P}\mathbf{A}_{\boldsymbol{\xi}} + \mathbf{C}_{\mathbf{d}}^\top \mathbf{C}_{\mathbf{d}} & \mathbf{P}\mathbf{B}_{\mathbf{u}} & \mathbf{P}\mathbf{B}_{\mathbf{d}} \\ \mathbf{B}_{\mathbf{u}}^\top \mathbf{P} & \mathbf{0} & \mathbf{0} \\ \mathbf{B}_{\mathbf{d}}^\top \mathbf{P} & \mathbf{0} & -\gamma^2 \mathbf{I} \end{bmatrix} + \eta \begin{bmatrix} \mathbf{C}_{\boldsymbol{\xi}}^\top & \mathbf{0} & \mathbf{0} \\ \mathbf{0} & \mathbf{I} & \mathbf{0} \end{bmatrix} \boldsymbol{\Pi} \begin{bmatrix} \mathbf{C}_{\boldsymbol{\xi}} & \mathbf{0} & \mathbf{0} \\ \mathbf{0} & \mathbf{I} & \mathbf{0} \end{bmatrix} \prec \mathbf{0}, \tag{13}$$

then, the system (11) has an induced L_2 gain less than or equal to γ [23, Thm. 4]. Note that the feasibility of (13) also implies global asymptotic stability of (11).

B. Stability and Performance for Representative Controllers

For proportional-action-based controllers, (12) is feasible (which implies $\dot{V}(\widetilde{\boldsymbol{\xi}}) < 0$ for all $\widetilde{\boldsymbol{\xi}} \neq \mathbf{0}$), ensuring global asymptotic and exponential stability. Consequently, (13) is also feasible, providing an induced L_2 gain bound γ.

For controllers with integral-action, (12) is non-strictly feasible, yielding stability in the sense of Lyapunov, while (13) is infeasible. This result follows from analyzing the closed-loop system (11) in two scenarios. First, when the nonlinearity operates as $\widetilde{\mathbf{u}} = \widetilde{\boldsymbol{\Phi}}(\widetilde{\mathbf{y}}) = \widetilde{\mathbf{y}}$, giving closed-loop dynamics $\dot{\widetilde{\boldsymbol{\xi}}} = \mathbf{A}_{\text{cl}} \widetilde{\boldsymbol{\xi}}$ with $\mathbf{A}_{\text{cl}} = \mathbf{A}_{\boldsymbol{\xi}} + \mathbf{B}_{\mathbf{u}} \mathbf{C}_{\boldsymbol{\xi}}$. If the controller for the dual variable $\boldsymbol{\lambda}$ has the structure $\mathbf{A}_{\boldsymbol{\lambda}} = \mathbf{0}$ as described in Section III-C for equilibria to satisfy KKT conditions, then $\mathbf{A}_{\text{cl}}$ is necessarily singular. To verify this, let $\widetilde{\boldsymbol{\xi}} = \begin{bmatrix} \mathbf{0}^\top & \mathbf{0}^\top & \mathbf{0}^\top & \mathbf{w}_{\boldsymbol{\lambda}}^\top \end{bmatrix}^\top$, with $\mathbf{w}_{\boldsymbol{\lambda}} \neq \mathbf{0}$. Then $\mathbf{A}_{\text{cl}} \widetilde{\boldsymbol{\xi}} = \begin{bmatrix} \mathbf{0}^\top & \zeta\,(\mathbf{H}^\top \mathbf{w}_{\boldsymbol{\lambda}})^\top & \mathbf{0}^\top & \mathbf{0}^\top \end{bmatrix}^\top$ where $\zeta \in \mathbb{R}$. Since $\mathbf{H}$ is not full row rank, its null space satisfies $\ker(\mathbf{H}^\top) \neq \{\mathbf{0}\}$; thus there exists $\mathbf{w}_{\boldsymbol{\lambda}} \in \ker(\mathbf{H}^\top)$ with $\mathbf{w}_{\boldsymbol{\lambda}} \neq \mathbf{0}$ such that $\mathbf{H}^\top \mathbf{w}_{\boldsymbol{\lambda}} = \mathbf{0}$. Therefore, $\mathbf{A}_{\text{cl}} \widetilde{\boldsymbol{\xi}} = \mathbf{0}$ for some $\widetilde{\boldsymbol{\xi}} \neq \mathbf{0}$, which implies that $\mathbf{A}_{\text{cl}}$ is singular. Second, when the nonlinearity operates as $\widetilde{\mathbf{u}} = \mathbf{0}$, we have $\dot{\widetilde{\boldsymbol{\xi}}} = \mathbf{A}_{\text{cl}} \widetilde{\boldsymbol{\xi}}$ with closed-loop matrix $\mathbf{A}_{\text{cl}} = \mathbf{A}_{\boldsymbol{\xi}}$. Since $\mathbf{A}_{\boldsymbol{\xi}}$ is Hurwitz, $\mathbf{A}_{\text{cl}} \widetilde{\boldsymbol{\xi}} = \mathbf{0}$ only when $\widetilde{\boldsymbol{\xi}} = \mathbf{0}$.

Given that the non-strict LMI (12) ensures $\dot{V}(\widetilde{\boldsymbol{\xi}}) \le 0$ globally with $\dot{V}(\widetilde{\boldsymbol{\xi}}) = 0$ (for $\widetilde{\boldsymbol{\xi}} \neq \mathbf{0}$) when $\widetilde{\boldsymbol{\xi}} = \mathbf{0}$ holds for both scenarios above, trajectories converge to the largest invariant set contained in $\mathcal{S} := \{\widetilde{\boldsymbol{\xi}} \mid \dot{V}(\widetilde{\boldsymbol{\xi}}) = 0, \begin{bmatrix} \widetilde{\mathbf{y}}^\top & \widetilde{\mathbf{u}}^\top \end{bmatrix}^\top \boldsymbol{\Pi} \begin{bmatrix} \widetilde{\mathbf{y}}^\top & \widetilde{\mathbf{u}}^\top \end{bmatrix} = 0\}$ via LaSalle's Invariance Principle [21, Thm. 4.4]. This set corresponds to the manifold associated with the singular closed-loop dynamics $\mathbf{A}_{\text{cl}} \widetilde{\boldsymbol{\xi}} = \mathbf{0}$. The non-strict ($\preceq \mathbf{0}$) feasibility of LMIs in optimization problems where the number of constraints exceeds the number of optimization variables has been previously discussed in [24, Sec. 5.6.3] and [25, cf. after Rem. 2].

V. Simulation Results

The proposed control architecture is validated on a single-area 14-bus power system with a ring topology (edge weight 6) and four additional edges (edge weight 1) between buses $(1, 5)$, $(3, 8)$, $(6, 12)$, and $(9, 14)$. The system parameters are $\mathbf{M}_i \in [7, 13]$, $\mathbf{D}_i \in [1.7, 2.3]$, $\boldsymbol{\Gamma}_i \in [0.35, 0.65]$, $\mathbf{R}_i \in [-0.065, -0.035]$. The AGC time constant is $\tau_{\text{z}} = 1$ s, $\boldsymbol{\alpha}_i = 1/14, \forall i \in \mathcal{N}$, and $\beta = -1$. The primal-dual dynamics with PI controllers (Section III-D) use parameters $\gamma_\rho = \gamma_\nu = \gamma_\lambda = 0.1, \sigma_\nu = \sigma_\lambda = 5$, and $\mu = 0.19$. We set $\mathbf{Q} = 0.01\mathbf{I}$ and $\mathbf{q} = \mathbf{0}$.

The LMI-based conditions (12)–(13) are analyzed using `YALMIP` with the `MOSEK` solver in MATLAB. For the above parameters, we verify that $\mathbf{A}_{\boldsymbol{\xi}}$ is Hurwitz, confirming the assumption in Section IV-A. Figure 3 shows time-domain simulation results obtained using the `ode45` solver in MATLAB to simulate the plant (1)–(2) and the controller (9)–(10). Bus 5 experiences a load increase of 0.1 pu at time $t = 5$ s. We compare the conventional ED with load-forecast $\delta = \mathbb{1}^\top \mathbf{d} + 0.3 \sin(2t)$, representing persistent forecast errors, to the proposed architecture with AGC state feedback for real-time load estimation. The area frequency decreases following the load increase until AGC restores frequency in both architectures, as seen in Figs. 3(a) and 3(b). This result illustrates a similar transient response for $\tau_{\text{z}} = 1$ s, primarily governed by the plant dynamics (1)–(2). Figures 3(c) and 3(d) show steady-state tracking error quantifying deviation from economic optimality. Due to persistent load forecasting errors, the conventional architecture exhibits deviation from the optimal steady state (Fig. 3(c)). In contrast, the proposed architecture is independent of load forecast errors

979-8-3315-8138-1

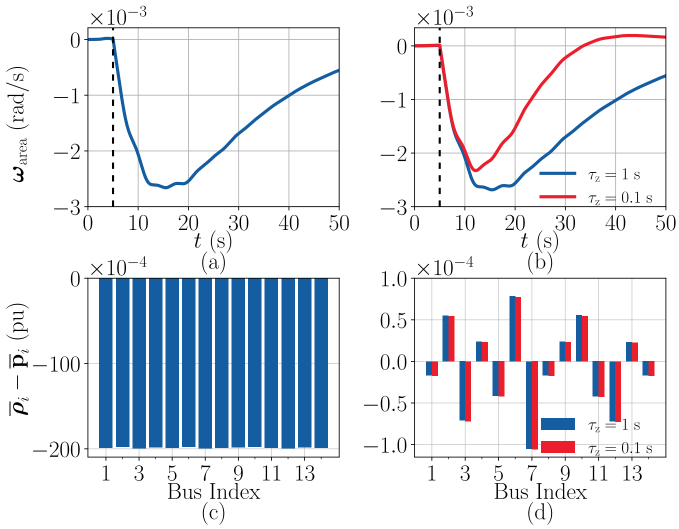

Fig. 3: Comparison of conventional (left) and proposed (right) architectures. (a),(b) Area frequency response under load transient. (c),(d) Steady-state tracking error.

and achieves economic optimality with near-zero steady-state error (Fig. 3(d)); both $\tau_z = 1$ s and $\tau_z = 0.1$ s converge to the same KKT equilibria (7). Consequently, as evident from Figs. 3(b) and 3(d), the proposed architecture provides the additional benefit of enabling faster AGC response (e.g., $\tau_z = 0.1$ s; this small value, while not typical in practice, is selected for illustration), achieving economic optimality at steady state without compromising stability.

VI. Conclusions and Future Work

We propose a control architecture for continuous-time ED and AGC that uses the AGC state as a proxy for real-time load demand. The continuous-time dynamics solve the integrated ED–AGC optimization problem in real-time, with equilibria shown to satisfy KKT optimality conditions. Stability guarantees are established via LMI-based conditions. Simulations on a 14-bus power system in MATLAB demonstrate that the control architecture maintains economic optimality at steady state while regulating frequency under load changes. Limitations include transient violations of generation capacity constraints and the lack of asymptotic or exponential stability for controller realizations that incorporate integral action. Future work includes extending the control architecture to a multi-area power system and high-fidelity EMS simulations.

Acknowledgment

Funding support from the Electric Power Research Institute under contract ID 10016671 and the National Science Foundation under Award 2305432 is gratefully acknowledged. The authors express their gratitude to Professor Murti Salapaka for insightful discussions and comments.

References

[1] D. Cai, E. Mallada, and A. Wierman, "Distributed optimization decomposition for joint economic dispatch and frequency regulation," *IEEE Trans. Power Syst.*, vol. 32, no. 6, pp. 4370–4385, 2017.

[2] P. Chakraborty, S. Dhople, Y. C. Chen, and M. Parvania, "Dynamics-aware continuous-time economic dispatch and optimal automatic generation control," in *Amer. Control Conf.*, 2020, pp. 1292–1298.

[3] S. Baros, Y. C. Chen, and S. V. Dhople, "Examining the economic optimality of automatic generation control," *IEEE Trans. Power Syst.*, vol. 36, no. 5, pp. 4611–4620, 2021.

[4] M. K. Singh, D. Venkatramanan, S. Dhople, B. Kroposki, and G. B. Giannakis, "Unifying energy-management problems for inverter-based power networks," *IFAC Pap. Online*, vol. 55, no. 13, pp. 282–287, 2022.

[5] B. Chen, R. Khatami, A. Al-Digs, and Y. C. Chen, "Incorporating system frequency dynamics into real-time locational marginal pricing of electricity," *IEEE Trans. Power Syst.*, vol. 39, no. 2, pp. 4638–4649, 2024.

[6] R. Khatami, M. Parvania, C. Chen, S. S. Guggilam, and S. V. Dhople, "Dynamics-aware continuous-time economic dispatch: A solution for optimal frequency regulation," in *Proc. Hawai'i Int. Conf. Syst. Sci.*, Hawaii, USA, 2020, pp. 1–10.

[7] D. Apostolopoulou, P. W. Sauer, and A. D. Domínguez-García, "Automatic generation control and its implementation in real time," in *Proc. Hawai'i Int. Conf. Syst. Sci.*, 2014, pp. 2444–2452.

[8] A. Sajadi, R. W. Kenyon, and B. Hodge, "Synchronization in electric power networks with inherent heterogeneity up to 100% inverter-based renewable generation," *Nat. Commun.*, vol. 13, no. 1, May 2022.

[9] S. V. Dhople, Y. C. Chen, A. Al-Digs, and A. D. Domínguez-García, "Reexamining the distributed slack bus," *IEEE Trans. Power Syst.*, vol. 35, no. 6, pp. 4870–4879, 2020.

[10] M. K. Singh, D. Venkatramanan, and S. Dhople, "Towards optimal primary- and secondary-control design for networks with generators and inverters," in *Annu. Allerton Conf. Commun., Control, Comput.*, 2022, pp. 1–6.

[11] S. Boyd and L. Vandenberghe, *Convex Optimization*. Cambridge, UK: Cambridge University Press, 2004.

[12] J. Nocedal and S. J. Wright, *Numerical Optimization*, 2nd ed. New York: Springer, 2006.

[13] A. Jokic, M. Lazar, and P. P. J. van den Bosch, "On constrained steady-state regulation: Dynamic KKT controllers," *IEEE Trans. Autom. Control*, vol. 54, no. 9, pp. 2250–2254, 2009.

[14] M. Kim and A. A. Adegbege, "Constrained primal-dual dynamics for QCQP with applications to economic dispatch," *IFAC Pap. Online*, vol. 50, no. 2, pp. 215–220, 2017.

[15] A. A. Adegbege, "Incrementally passive primal-dual dynamics for real-time optimization," in *Amer. Control Conf.*, 2019, pp. 1767–1772.

[16] V. Cerone, S. M. Fosson, S. Pirrera, and D. Regruto, "A feedback control approach to convex optimization with inequality constraints," in *IEEE Conf. Decis. Control*, 2024, pp. 2538–2543.

[17] K. Sawant, P. Seiler, M. R. Jovanović, J. Poon, and S. Dhople, "Real-time solution strategy for linearly constrained quadratic programs with proportional-integral control and variants," in *Amer. Control Conf.*, 2025, pp. 910–917.

[18] G. Qu and N. Li, "On the exponential stability of primal-dual gradient dynamics," *IEEE Control Syst. Lett.*, vol. 3, no. 1, pp. 43–48, 2019.

[19] A. Hauswirth, Z. He, S. Bolognani, G. Hug, and F. Dörfler, "Optimization algorithms as robust feedback controllers," *Annu. Rev. Control*, vol. 57, p. 100941, 2024.

[20] A. A. Adegbege and M. Y. Kim, "Saddle-point convergence of constrained primal-dual dynamics," *IEEE Control Syst. Lett.*, vol. 5, no. 4, pp. 1357–1362, 2021.

[21] H. Khalil, *Nonlinear Systems*, 3rd ed. Upper Saddle River, NJ, USA: Prentice Hall, 2002.

[22] B. Hu and P. Seiler, "Exponential decay rate conditions for uncertain linear systems using integral quadratic constraints," *IEEE Trans. Autom. Control*, vol. 61, no. 11, pp. 3631–3637, 2016.

[23] H. Pfifer and P. Seiler, "Integral quadratic constraints for delayed nonlinear and parameter-varying systems," *Automatica*, vol. 56, pp. 36–43, 2015.

[24] A. Jokic, "Price-based optimal control of electrical power systems," PhD thesis, Technische Universiteit Eindhoven, Dept. of Electrical Engineering, 2007.

[25] M. Colombino, E. Dall'Anese, and A. Bernstein, "Online optimization as a feedback controller: Stability and tracking," *IEEE Trans. Control Netw. Syst.*, vol. 7, no. 1, pp. 422–432, 2020.